Thermal Science and Engineering Progress 62 (2025) 103651

Contents lists available at ScienceDirect

Thermal Science and Engineering Progress

journal homepage: www.sciencedirect.com/journal/thermal-science-and-engineering-progress

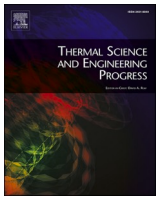

Thermochemical valorization of biomass into sustainable biomaterials and biofuels: The potential of AAEMs rich mediterranean wastes☆

Assia Maaoui [a,b,*], Raouia Chagtmi [a,b], Francesca Cerciello [b], Aida Ben Hassen Trabelsi [a], Fernando Stanzione [b], Maria Maddalena Oliano [b], Osvalda Senneca [b], Barbara Apicella [b]

[a] Laboratory of Wind Energy Control and Waste Energy Recovery, LMEEVED, Research and Technology Centre of Energy, CRTEn, B.P. 95, 2050 Hammam-Lif, Tunisia
[b] Istituto di Scienze e Tecnologia per l'Energia e la Mobilità Sostenibili (STEMS)-CNR, 80125 Napoli, Italy

ARTICLE INFO

Keywords:
Pyrolysis
Co-pyrolysis
Lignocellulosic biomass
Biochar
Bio-oil
Synergetic effects

ABSTRACT

Mediterranean biomass presents distinctive features compared to the Northern lignocellulosic biomasses, which are typically exploited for thermochemical conversion. The present work addresses slow pyrolysis and co-pyrolysis of three biomass largely available in the Mediterranean regions, namely cactus cladodes (CC), pomegranate peels (PGP) and pine cones (PC) in a fixed bed batch. Notably, CC, is characterized by a large content of ashes (>20 %), and is particularly rich in alkali and alkaline-earth metals (AAEMs), which, upon co-pyrolysis, could act as catalysts and affect the chemical composition of the bio-oil, as well as the properties and yields of the biochar.

The results indicated that co-pyrolysis decreases the gas yield and increases the bio-oil and biochar yields.

The bio-oils produced from either PGP or PC are complex mixtures of chemicals, including phenols, aromatics, aliphatics and anhydrosugars. Co-pyrolysis of PC with CC increases the content of phenol and aromatics in the bio-oil, while decreases the content of retene derivatives. Co-pyrolysis of PGP with CC increases the content of phenols and reduces that of furfural and anhydrosugars.

The biochars produced from co-pyrolysis of CC with either PGP or PC have low O/C and H/C ratios, high alkalinity and large content of Ca, K, Mg and P.

1. Introduction

Energy transition is currently one of the most important challenges of mankind. Fossil fuels at present sustain 53 % of the global demand of electricity, 66 % of the industrial heat consumption and up to 98 % of the demand of transport fuels [1]. In the near future, biomass is expected to play a very important role as a source of renewable energy and chemicals [1,2]. It has indeed been estimated that in 2050 between 15 and 50 % of the global energy demand will come from biomass [3]. In this regard, biomass, especially lignocellulosic biomass, can be considered the most suitable renewable energy source for fuel production [3]. Lignocellulose biomass is rich in carbon and contains negligible content of other undesirable elements, such as nitrogen and sulphur [4].

Identifying suitable biomass species and technologies that can provide high-energy outputs and replace conventional fossil fuels has been the focus of many researchers in recent years [5,6]. Several alternative routes have been proposed for the conversion of biomass, including thermochemical and biochemical processes. Thermochemical conversion is one of the most promising pathways for biomass conversion, in particular, pyrolysis has highly desirable attributes, including the ability to produce concurrently valuable solid, liquid, and gaseous products [5,7]. As pointed out in several studies, pyrolysis conditions and reactor technologies, in particular temperature, heating rate, residence time, particle size, etc., affect the yields and physicochemical properties of the final products [7,8]. For example, slow pyrolysis is the preferable method for the production of high quantities of char, while fast pyrolysis promotes the yield of oil and flash pyrolysis is recommended if the target is pyrolysis gas.

The most convenient pyrolysis route depends, therefore, must take inti account the main target, as well as other issue such as the plant and operational cost, the complexity of the technology involved, the easiness of storage and transportation [9]. Pyrolysis in fixed bed reactors of small

☆ This article is part of a special issue entitled: 'INFUB 14' published in Thermal Science and Engineering Progress.

* Corresponding author.
E-mail address: maaouiessia002@gmail.com (A. Maaoui).

https://doi.org/10.1016/j.tsep.2025.103651
Received 17 January 2025; Received in revised form 10 April 2025; Accepted 4 May 2025
Available online 5 May 2025

to medium scale appears particularly convenient for valorization of wastes of the agro-industry in African and Mediterranean regions, on one side because of the relatively low complexity and cost of this technology, on the other side because this type of pyrolysis conditions are favourable for production of biochars, which can be advantageously exploited to amend dry and scarcely fertile soils.

Co-pyrolysis of different feedstocks, catalytic pyrolysis and catalytic co-pyrolysis have also received much interest from researcher groups worldwide [10,11] as ways to improve the quality of the products. Studies focused either on the co-pyrolysis of biomass with plastic wastes [12–14], or on co-feeding of different lignocellulosic biomass [15–18] and highlighted how synergistic effect can affect the products [19,20]. The main effects reported in some recent papers are summarised in (Table 1). Usino et al. [15] reported synergetic effect between palm kernel shell and sawdust biomasses in terms of pyrolysis reaction mechanisms, including dehydration, decarboxylation, and restructuring of methoxy groups and long-chain carbon bonding. Authors showed that it is possible to enhance the production of some valuable compounds by tuning the biomass composition and blend ratio. Several papers addressed, in particular, the role of the alkali and alkaline earth metals (AAEMs) present in biomass during pyrolysis and co-pyrolysis and reported synergetic and catalytic effects which modify the [15,21–23] yields and chemical composition of bio-oil and bio-gas, but also of biochar [24,25], indeed biochars with high concentrations of AAEMs are likely to have a high pH and, if used as soil fertilizers, could have a liming effect [26]. However, a clear understanding of the relation between AAEMs and biomass structure and origin is, in fact, still missing, and the effects of AAEMs rich biomass with mixtures of different biomass deserve accurate investigation.

The present work focuses on pyrolysis and co-pyrolysis of some waste biomasses of the Mediterranean region, which have not received as much attention in previous literature as the lignocellulosic biomasses largely used in Northern Europe. These Mediterranean biomasses have interesting and peculiar properties, which deserve investigation. The first biomass, cactus cladodes (CC), is a spontaneous plant covering, only in Tunisia, the remarkable area of 600.000 ha. Cactus cladodes can be exploited in co-pyrolysis because they are rich in AAEMs, in particular calcium (Ca), potassium (K) and magnesium (Mg). The second biomass waste is Pine Cones (PC). Pines cover around 20000 ha of Tunisian planted area and have lignocellulosic structure similar to that of the many wooden biomasses of the Northern hemisphere. The third biomass waste is pomegranate peels (PGP). Pomegranate cultivation covers around 13.500 ha of Tunisian planted area and is quite different from traditional lignocellulosic biomasses. In terms of production, Tunisia is one of the most important pomegranates producing countries with about of 75,000 tons/year in 2019 and mainly located in Gabès, South-East Tunisia. This region contains 35 % of the national pomegranate producers in Tunisia [27]. Pomegranate peel, makes up approximately 40–50 % of the total weight of pomegranate. This biomass is rich in functional groups such as carboxylic, hydroxyl, and lactone groups due to its high content of polymers that include cellulose, hemicellulose, and lignin [28–32]. It is an excellent source of phenolic compounds, protein and bioactive peptides and polysaccharides [33,34].

2. Materials and methods

2.1. Pyrolysis experiments

Cactus cladodes (CC), pomegranate peels (PGP) and pinecones (PC) wastes were dried and crushed to reduce the particle size to a range of 1–3 mm.

Slow pyrolysis and co-pyrolysis experiments were conducted in a vertical tubular reactor, whose scheme is reported in (Fig. 1) [39], which has been already presented in detail in previous papers. It consists of a quartz tube of internal diameter of 2 cm externally heated by an electrical furnace. Approximately 1 g of sample are positioned in the central

Table 1
Previous studies on biomass co-pyrolysis.

Biomass	Conditions	Results	Reference
Cactus cladodes/ Pinecones-Pomegranate peels	Slow pyrolysis/co-pyrolysis (500 °C)	−Increase in bio-oil yields and the decrease of gas yield. −biochars rich AAEMs. −Improvement in bio-oil composition.	This study
Sewage sludge/ Pinewood sawdust	Fast co-pyrolysis (500 °C)/ ratio 1:1	−Improvement of the composition of the bio-oil −Enhancement of gas production by the catalytic effect of the ash in the sewage sludge. −Char with high nutrient content	[35]
Sawdust and hardwood biomass/Plastic	Slow pyrolysis/co-pyrolysis (300, 400 and 500 °C)/ 20 wt % of plastic blend	−Synergetic effects among the biomass components. −Improvement of biochar properties −Decrease in biochar yields after plastic addition at 400 and 500 °C	[36]
Bamboo and oak wood/Plastics	Slow co-pyrolysis (500 °C)/ 10 and 20 wt% of plastic blends	−Reduction in the yield of char and CO_2 and enhancement in the yield of H_2 and some hydrocarbon gases. −Higher liquid product yield and improvement of HHV for both oil and char. −Increment of hydrocarbon gases content and decline in the CO and CO_2 contents	[12]
Wood sawdust/ Plastics	Slow co-pyrolysis (500 °C)/ 30, 50 and 80 wt% of plastic blends	−Decrease in char yield with improvement of its properties (carbon content, heating value, bulk density and electrical conductivity) and reduction in the oxygen content and surface area.	[37]
Corn stalks, wheat straws and pine sawdust/Poultry manure	Slow pyrolysis/co-pyrolysis (550 °C)	−Improvement in biochar HHV and the surface area. −Improvement in bio-oil quality in terms of viscosity, HHV and ash content. −High concentration of CH_4, H_2 and C2–4	[38]
Palm kernel shell/ mahogany or iroko sawdust	Fast co-pyrolysis (600 °C and 5 s)/ Different blend ratio (1:1/ 1:1:1/ 1:2:2/ 2:1:1)	−Interaction during the co-pyrolysis of different biomasses. −Effect of the biomass type/composition and blend ratio. −Decrease in the relative yield of the phenols depending on blend ratio.	[15]
Rubberwood sawdust/ Sewage sludge	Pyrolysis/co-pyrolysis (450, 500 and 550 °C/ Different blend ratio (25:75, 50:50 and 75:25 wt%)	−Increment of the liquid product and reduction in the solid yield. −Production of biochar with higher carbon	[24]

(continued on next page)

Table 1 (*continued*)

Biomass	Conditions	Results	Reference
		content and inorganic elements.	

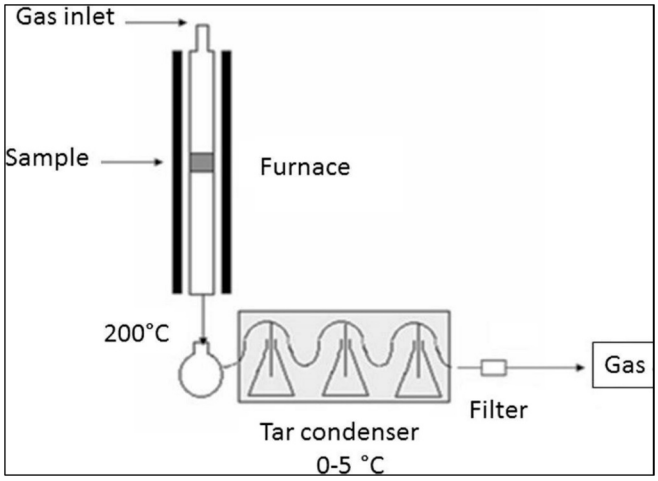

Fig. 1. Schematic of pyrolysis fixed bed reactor used in pyrolysis/co-pyrolysis experiments [39].

region of the reactor. A downward flow of N_2 (250 mL/min) drives the volatile pyrolysis products through a train of ice cooled condensers at −5°C and a fabric filter. The sample temperature is monitored by a thermocouple and the heating program is set to achieve heating rates of 10 °C/min up to a final temperature of 500 °C, followed by an isothermal step of 60 min. Experiments were carried out with approximately CC, PGP or PC and with 1:1 mixtures of CC with PGP and CC with PC.

Biochar was recovered after the pyrolysis experiments at room temperature. The bio-oil was recovered from the flasks by acetone washing. The weight of the fabric filter was measured before and after each test to ensure that all condensable products are accounted for in the mass balance.

The yields of the liquid and solid fractions were calculated based on the following equations (Eq. (1)) and (Eq. (2)):

$$\text{Biochar yield (wt\%)} = \frac{\text{weight of } Biochar\,(g)}{raw\ feedstock\,(g)} * 100 \quad (1)$$

$$\text{Bio} - \text{oil yield (wt\%)} = \frac{\text{weight of } Bio - \text{oil}(g)}{raw\ feedstock\,(g)} * 100 \quad (2)$$

The pyrolytic gas yield was calculated by subtraction (Eq. (3)):

$$\text{Gas yield (wt\%)} = 100 - (\text{Bio} - \text{oil (wt\%)} + \text{Biochar (wt\%)}) \quad (3)$$

An array of analytical techniques were used to further characterize bio-oil and biochars, and these will be discussed in the paragraphs that follow.

2.2. Analyses of biomass and pyrolysis products

Biomasses and biochar samples have been characterized in terms of proximate (TGA Q500IR thermogravimetric analyser) and ultimate analyses (LECO CHNS-932 elemental analyser), mineral composition, FTIR spectroscopy (spectrophotometer type Bruker Vertex 80 V series) and XRD analysis (PANalytical X'Pert Pro X-ray diffractometer) with diffraction angle of 10–80°. Both XRD and FTIR analyses were carried out in triplicate and the detailed measurement conditions can be found elsewhere [20].

Proximate analyses of CC, PC and PGP samples and their corresponding biochars were conducted in an inert gas (N_2) with a flow rate of 50 mL/min. The TGA process includes an isothermal period of one minute at 50 °C for system equilibration, followed by a ramp of 15 °C/min to 800 °C, which is maintained at this temperature for ten minutes. The weight loss during this period, corresponding to the VM and the moisture content, was determined by the weight loss between 50 and 105 °C. The inert gas was then substituted by an airflow rate of 20 mL/min at the same temperature for 5 min, which caused the combustion of the FC and allowed the quantification of the ashes.

Mineral content of the biochar samples was assessed using the Agilent ICP-MS 7500 spectrometer. 0.1 to 0.2 g of biochar was treated with 4 mL deionized water, 5 mL aqueous solution of HNO_3 (65 % by weight) and 1 mL aqueous solution of H_2O_2 (30 % by weight) for 30 min by microwave heating (final temperature equal to 180 °C). ICP-MS analysis was carried out on the digested sample after filtration and dilution with demineralized water to a volume of 50 mL. All the analyses were conducted in triplicate.

The high calorific value (HHV) of the biomass and biochars samples has been assessed based on the proximate analysis results. HHV, thermal stability (*Ts*) and Fuel ratio (*Fr*), indices have been defined according to Eq. (4)–(6). These indices are considered the basis for evaluating the quality of biochar as an energy source [40,41].

$$\text{HHV}\left(\text{MJ kg}^{-1}\right) = -0.3675 + 0.3137\,\text{C} + 0.7009\,\text{H} + 0.0318\,\text{O} \quad (4)$$

$$\text{Thermal stability (Ts)} = \frac{FC\ of\ biochar}{(FC + VM)\ of\ biochar} \quad (5)$$

$$\text{Fuel ratio (Fr)} = \frac{FC\ of\ biochar}{VM\ of\ biochar} \quad (6)$$

Where FC and VM are fixed carbon content and volatile matter content (wt%, dry basis) of solid fuel sample.

The pH and EC values of the biomasses and biochar samples (sample: distilled water = 1:20, w/v) were measured with a pH-meter (Proline Plus, Mettler-Toledo GmbH, Switzerland) equipped with an electrode (QP2111T-pH-electrode) and an EC meter (QC2260T-EC-electrode). The solution was agitated for 24 h to reach equilibrium before pH and EC analysis.

Bio-oil was analysed using Gas chromatography-mass spectrometry (GC–MS) (AGILENT GC 6890−MSD 5975C). In the GC, a HP-35 (length 30 m, i.d. 250 μm, film 0.25 μm) column is mounted. Bio-oil sample injection was done in split less mode at 573 K with a gas flow of 1 mL/min (STP). The temperature program consisted of four isothermal steps: 323 K (5 min), constant heating for 30 min to 473 K (5 min), constant heating for 1.75 min to 543 K (5 min) and finally, constant heating for 6 min to 573 K (15 min). The transfer line between the GC and the MS was held at 573 K. The mass spectrometer operated in electron ionization mode scanning *m/z* from 50 to 400. The identification of the compounds was performed according to the NIST database.

3. Results and discussion

3.1. Biomass characterization

Results of the physicochemical properties of the used biomasses for the pyrolysis process are illustrated in Table 2. According to Table 2, all biomasses cactus cladodes (CC), pomegranate peels (PGP) and pinecones (PC) are characterized by low moisture content (less than 10 wt %). Biomass with low moisture content is preferable for thermal conversion, as moisture levels below the permissible limit (<10 %) indicate excellent raw material suitability for energy production. A significant content of VM is observed for all samples with values over 60 wt%. The high VM content of a biomass indicates its suitability for bio-oil production through pyrolysis [42]. On the other hand, the residual VM

Table 2
Main properties of biomass samples.

	CC	PGP	PC
Proximate analysis (wt%)			
Moisture	2.26	2.9	4.0
VM	64.3	66.0	64.4
FC	8.2	28.7	24.9
Ash	25.3	2.3	6.7
Ultimate analysis (wt%)			
C	34.1	49.9	54.5
H	4.6	6.34	6.6
N	1.0	0.85	0.94
S	0.13	0.00	0.09
O*	34.8	40.6	31.1
pH	5.5	4.9	7.2
EC (mS/cm)	5.5	1.6	0.30
Fuel properties			
HHV(MJ/kg)	12.0	17.0	20.5
H/C	1.6	1.5	1.4
O/C	0.76	0.61	0.43
Fuel ratio (*Fr*)	0.13	0.43	0.39
Thermal stability (*Ts*)	0.11	0.30	0.28
Mineral composition (wt%)			
CaO	48.2	8.6	22.3
MgO	7.1	1.5	3.7
K_2O	11.6	47.9	9.1
Na_2O	0.46	1.1	1.7
P_2O_5	0.94	2.8	2.2
Cl	5.8	7.5	0.18
Fe_2O_3	1.8	0.06	3.3
Al_2O_3	1.2	0.53	7.2
SiO_2	10.2	0.50	32.8

(*) by difference.

content of biochar can have a direct influence on C and N dynamics in soil.

It can be observed, that the VM content of used biomasses in this study is lower or greater than other values using the same feedstocks reported in several studies [43–47]. The geographical location, local ecosystem, cultivation conditions, as well as the surrounding environment might explain these variations.

The ash contents of PGP (2.34 wt%) and PC (6.73 wt%) were significantly lower than that of CC (25.27 wt%). In general, ash fraction contains AAEMs, which affect the thermal degradation pathway of biomass [48]. For example, Mahadivan et al. [48] observed that the thermal decomposition of lignocellulosic biomass is affected significantly by the presence of AAEMs, which enhanced the breakdown of the polymeric structure of cellulose and lignin affecting the yield of char, gas and volatiles. AAEMs in biomass in particular alkali metals (K and Na) and alkaline earth metals (Ca and Mg) have a catalytic effect during pyrolysis [11,49,50], in contrast, a high ash content results in lower HHV and can pose operational problems in combustion, such as slag formation and corrosion within the furnace chamber, which decrease the conversion efficiency [51,52].

From Table 2, it can be observed also that the FC content is 8.16, 24.89 and 28.70 wt% for CC, PC and PGP, respectively. Typically, the high FC content increases biochar production during pyrolysis process. The elemental analysis shows high carbon and hydrogen contents for PC (54.53 and 6.56 wt%) and PGP (49.89 and 6.34 wt%). However, CC sample has a low C content (34.15 wt%) compared to other residues reported in the literature such as cactus peels [19], mango leaves [53] and wood wastes [54]. All biomasses have low content of S and N (less than 0.3 % and around 1, respectively). As shown in Table 2, the HHV of the PGP and PC samples is 17.01 and 20.54 MJ/kg. The high values could be explained by the composition of the biomass in particular the lignin content. The HHV of PGP and PC samples is similar to other lignocellulosic wastes like gumweed (18.6 – 17.7 MJ/kg), pomegranate peels [43] and cassava rhizome (20.3 MJ/kg). However, the low HHV of CC biomass (12.01 MJ/kg) is explained by the low FC and high ash content, as illustrated by the proximate analysis (Table 2). This result is compared to banana peel wastes (12.4 MJ/Kg) reported by Abdullah et al. [55]. On the other hand, CC sample had low C and H contents and high O content, resulting in low HHV.

Regarding the atomic H/C and O/C ratios, Table 2 and Fig. 2 show that in a Van Krevelen diagram, the three selected biomasses are within the lignocellulosic biomass region, however CC has the highest O/C ratio, which is consistent with its high holocellulosic and sugar contents [20], while PC has the lowest O/C value, more consistent with a higher lignin content [54]. Due to the high H/C and O/C ratios of biomass, compared to fossil fuels, the bio-oils typically have lower heating value and are highly corrosive, which explains why hydrogenation upgrading processes are usually required. On the other hand, the higher H/C ratio and the presence of C—O functionalities increase the biochar stability and polarity.

CC and PGP biomasses are acidic with pH of 5.52 and 4.87, respectively, indicating the presence of organic acids like phenols and fatty acids in its structure.

According to the mineral matter composition (Table 2), the selected biomasses have different concentrations of inorganic elements. The mineral content confirms the abundance of AAEMs in CC feedstock, in particular Ca. The most abundant elements are in descending order Ca (48.16 wt%), K (11.58 wt), Si (10.18 wt%) and Mg (7.06 wt%). PGP contains in descending order of K (47.90 wt%), Ca (8.58 wt%) and Cl (7.54 wt%). PC is richest in Si (32.75 wt%), followed by Ca (22.30 wt%), K (9.10 wt%), Al (7.19 wt%), Mg (3.74 wt%). Other trace elements are also detected in all biomasses such as Na, P and Fe. The high content of AAEMs in CC makes it a very interesting candidate for the co-pyrolysis, because AAEMs may have a catalytic activity and promote chemical interactions between the primary pyrolysis products in the vapor phase [56].

FTIR spectra of CC, PGP and PC are shown in Fig. 3**a**. The peaks typical of cellulose, hemicellulose and lignin can be found in the spectra. The peak at 2856 cm^{-1} is associated to C—H stretching present in methylene group, hemicellulose, cellulose, pectin and lignin [57]. The peak at 1018 cm^{-1} is indicative of C—O stretching in both cellulose and hemicellulose and the presence of lignin is instead clearly shown by the

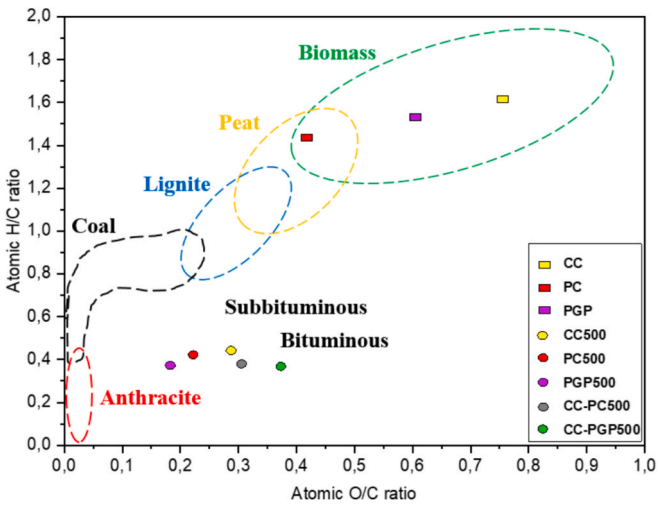

Fig. 2. Van Krevelen diagram for biomass samples and their derived biochars.

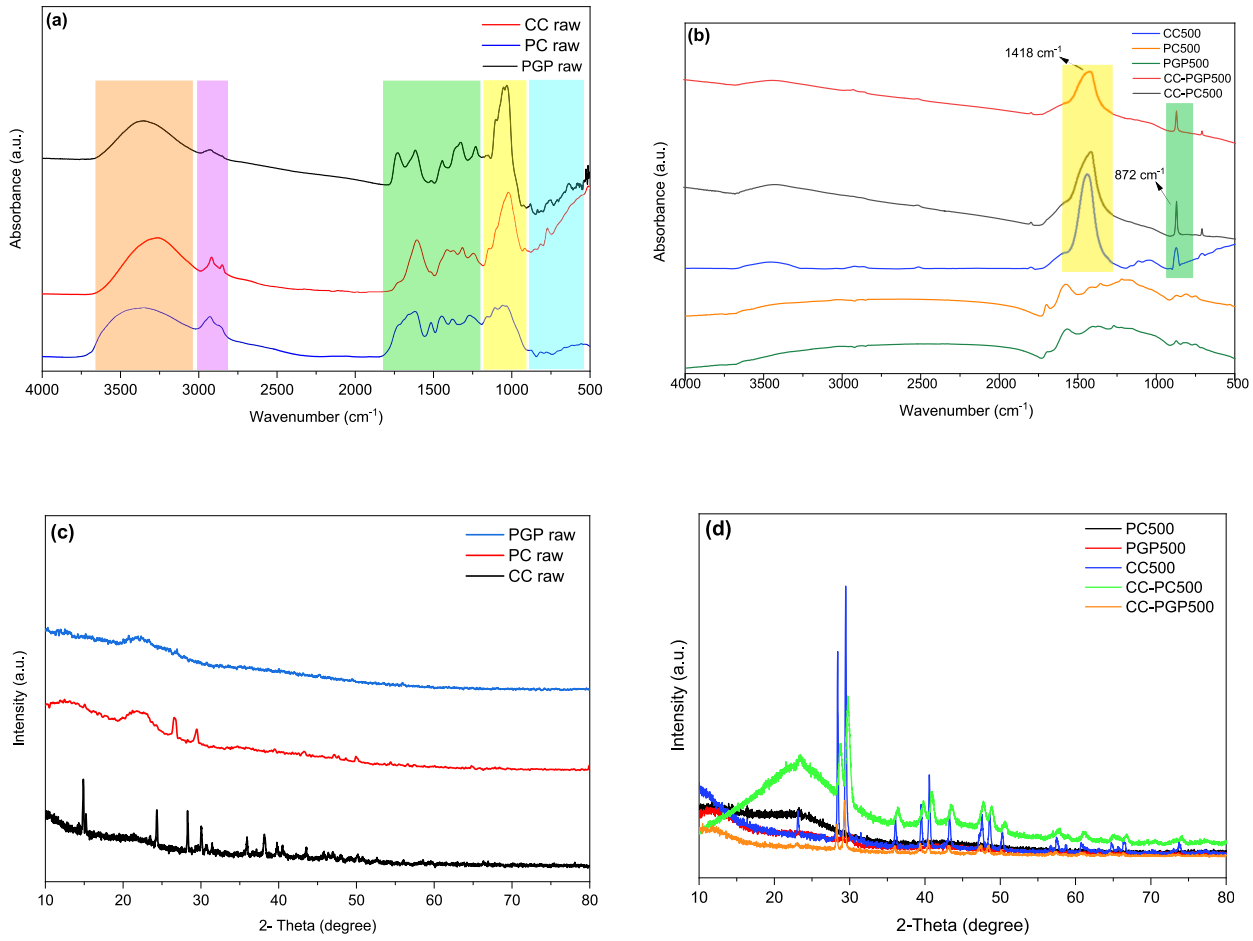

Fig. 3. FTIR and XRD spectra of biomass samples (a, c) and their obtained biochars (b, d).

peaks at 1614 cm^{-1} and 1521 cm^{-1} due to stretching of the O—H bonds of the phenolic and C═C groups of the aromatic skeletal mode, respectively [58,59]. Notably, the cellulose peak at 1018 cm^{-1} is the one with the most remarkable differences among the samples, decreasing in the order PGP, CC and PC [54].

Besides the presence of cellulose, hemicellulose and lignin, the FTIR spectra reveal other important features. For all samples, between 3600–3200 cm^{-1} a broad bump is observed, which may be caused by the overlapping of O—H vibration due to the presence of hydroxyl groups, carbohydrates and lignin [59]. The peak at 2920 cm^{-1} in the PC and CC is associated with the stretching vibration of aliphatic C—H groups and the peak around 1726 cm^{-1} represents the C═O stretching of the carbonyl group. In addition, at 782 cm^{-1}, a peak associated with C—H alkyne bends is observed, which is possibly related to complex molecules such as proteins and in the 877 – 633 cm^{-1} range C—H deformation of the aromatic ring is obvious [57]. The bands characteristic of C—O and Si—O stretching, are clearly visible between 1320 cm^{-1} and 1025 cm^{-1}, indicating the presence of aromatic proteins, phosphoric groups, and polysaccharides [60]. Notably, these bands are most evident in the CC and PGP samples [61].

XRD analysis has been used to identify the occurrence of various crystalline materials, which influence the properties of biochar in terms of its applications. The XRD patterns of PC, PGP and CC samples are illustrated in Fig. 3**c**. Some differences can be observed by comparing the selected samples. A broad peak at approximately 23.5° is observed in the XRD patterns of PC and PGP, resulting from the crystalline cellulose present in their structure. This peak can be ascribed to (002) planes of the cellulose but its position, anticipated with respect to graphite, along with its broadness, are clearly features of amorphous carbon [62]. The peaks at around 26.64°, 29.44° identified in the PC biomass are attributed to the presence of SiO_2 and $CaCO_3$, respectively. Compared to PC and PGP, more peaks are present in CC biomass. The XRD pattern shows ten major peaks at $2\theta = 14.88, 15.22, 24.33, 28.27, 30.20, 35.93, 38.17, 39.78, 40.48$ and 43.54, which correspond to the chemical structure of calcium oxalate monohydrate (whewellite) ($CaC_2O_4{\cdot}H_2O$) present in the CC feedstock [60,63]. This result is in good agreement with results reported by Rojas-Molina et al. [63] and Madera-Santana et al. [64], which reported also the presence of whewellite crystals in cactus cladodes.

TG and DTG curves of CC, PGP and PC samples under inert atmosphere with a heating rate of 10 °C/min are shown in Fig. 4. Important differences can be observed among the three samples and with the lignocellulosic biomasses from Northern countries, which are most typically investigated for pyrolysis in literature.

The TG-DTG profile of PC pyrolysis, which is among the investigated samples the only woody one, resemble those of several lignocellulosic biomasses reported in the literature such as pate palm waste [65], olive pomace [66], cascabela thevetia [67], rubber wood sawdust [68] and waste tobacco stem and corn stalk [69]. The first stage of mass loss is observed around 100 °C, due to release of moisture. Pyrolysis starts above 200 °C and ends by 500 °C. The DTG curve can be fitted by assuming the existence of three components, with peaks at 210, 290 and 334 °C. This is typically attributed to the co-existence in the biomass of hemicellulose, cellulose and lignin whose decomposition temperatures, according to the literature, fall in the ranges of 200–315, 315–400, and 160–700 °C, respectively [70]. Notably, a considerable degree of overlap exist between the DTG peaks, especially in the temperature range 250–350 °C. The long tail at temperatures around 450 °C is attributed to

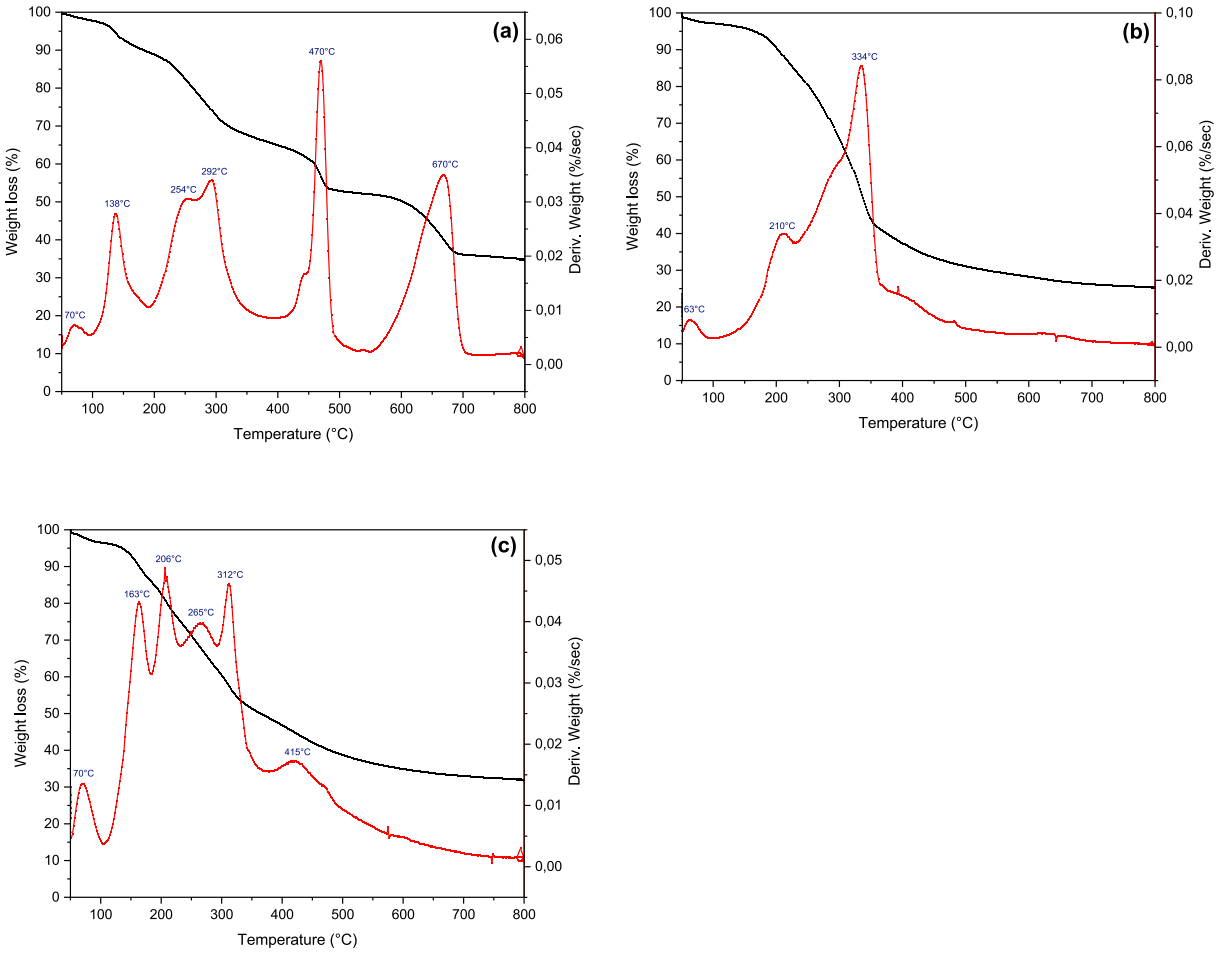

Fig. 4. Thermogravimetric analysis curves of (a) CC, (b) PC and (c) PGP samples at 10 °C/min.

lignin degradation.

In the case of CC and PGP samples, several peaks are observed, which are consistent with the complexity of biomass structure and composition already highlighted by FTIR analysis.

For PGP (Fig. 4**c)**, the weight loss observed below 200 °C can be attributed to elimination of water and very volatile compounds. Three consecutive peaks are then observed between 200 and 380 °C: the protruding peak between 200 and 240 °C can be attributed to degradation hemicellulose, pectin and the more lignin monomers [71]. The peak between 240 °C and 380 °C can be mainly associated with the degradation of cellulose and partly overlaps with further degradation of lignin, which indeed decomposes over a wide range of temperatures. A late peak occurs between 600 and 700 °C, which can be assigned to decomposition of inorganic matter such as metal carbonates [43].

The TG and DTG curves of CC stem out because peaks are much more resolved and separated than for the other biomasses (Fig. 4**b**): a first peak at 138 °C can be ascribed to the dehydration of free moisture and polysaccharides. Two peaks between 200 °C and 300 °C can be attributed to hemicellulose (at 254 °C) and cellulose (at 292 °C). A peak at 470 °C can be attributed to the thermal decomposition of carbohydrates, proteins, saccharides. San Miguel et al. [72] confirmed that decomposition of proteins and carbohydrates starts above 300 °C and 390 °C, respectively and that interactions between pyrolysis products occur at this stage with generation of gas [44,72]. Finally, another stage from 500 to 700 °C with an intense peak at 670 °C can be mainly attributed to the decomposition of $CaCO_3$ [73] and also thermal cracking of more stable substances, such as silicate, oxalates and chlorinated salts, polymeric organic substances, the poly-condensation of solid char and the production of some aromatic substances [53,72]. The CC and PGP thermogravimetric behavior is consistent with that of other wastes reported in the literature, including mango leaves [53] and municipal sludge [22].

3.2. *Biochar and bio-oil characterization*

3.2.1. *Products distribution*

Products yields obtained upon pyrolysis of the single biomass (CC500, PC500 and PGP500) and upon co-pyrolysis (CC-PC500 and CC-PGP500) are presented in Fig. 5**A and B**.

Many studies addressed the effects of chemical composition and ash fraction on products yield distribution [51,74]. For example, it has been reported that the presence of Ca in the ash fraction leads to a lower bio-oil and higher biochar yield [51] and that AAEMs may inhibit the diffusion of gases within biomass particles, thereby favouring cross-linking reactions and char formation. The results obtained for the single biomasses (CC, PC and PGP), which reported in Fig. 5**A**, show that CC has the highest biochar and gas yields, consistent with its high ash content (Table 2).

The yields obtained from pyrolysis experiment on the single biomasses (Fig. 5**A**) have been used to predict the yields of co-pyrolysis experiments, under the hypothesis that the biomasses present in the mixture do not interfere with each other so that the cumulative yields are the weight average of the single yields. These theoretical yields are reported in Fig. 5**B** as stars. It can be appreciated that the gas yields decrease, in favour of bio-oil, but the biochar yields remain approximately the same as the theoretical values, indicating no enhancement of pyrolysis rate and therefore no catalytic actions from the AAEMs rich CC.

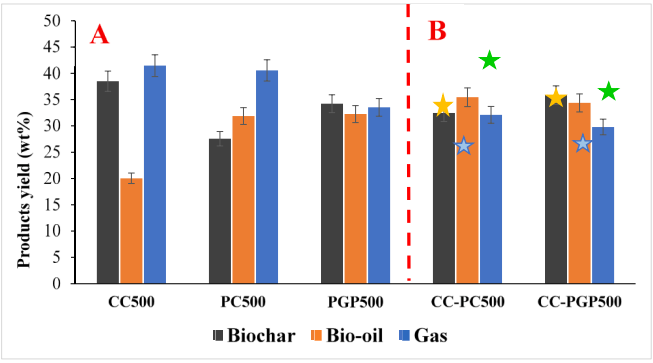

Fig. 5. Products yield distribution of pyrolysis: (A) pyrolysis of individual biomass; (B) co-pyrolysis (stars: theoretical results).

Actually the influence of AAEMs on the products quality and yields in the literature is not univocous, as it can be positive or even negative, depending on operating conditions [11,75], on biomass type and composition [51,76], on the content of proteins, lipids and carbohydrates [77]. For example, Alvarez et al. [35] conducted a study of fast co-pyrolysis of lignocellulosic biomass (pinewood sawdust) and sewage sludge and documented an enhancement of gas yield thanks to the catalytic effect of the ash forming species of sewage sludge. On the contrary, Chen et al. [78] conducted co-pyrolysis in a fixed bed reactor of nannochloropsis microalgae and bamboo waste and found a decrease of gas yield compared with pyrolysis of the single biomass, which they attributed to inhibition of secondary breakdown reactions of volatiles.

It must also be noted that pyrolysis has been carried out at 500 °C, therefore several minerals, remain in the solid sample, especially Ca, which remains in the form of carbonate catalytically inactive as CaO. Moreover, due to the downward flow of N_2 in the experimental set up, the contact time between the char and primary volatiles may be insufficient for secondary reactions between char and volatiles to take place.

3.2.2. Biochar characteristics

The main properties of the biochars obtained upon pyrolysis at 500 °C of single biomass or mixtures of CC-PGP500 and CC-PC500 are reported in Table 3. The values expected from co-pyrolysis in absence of synergistic effects (calculated as weight average of the results for single biomasses) are also reported in the Table 3.

It can be observed that CC500 biochar has the highest residual content of VM and lowest value of FC. This is due to the fact that VM calculation through proximate analysis includes the CO_2 fixed in $CaCO_3$, which decomposes above 600 °C, as shown by the TGA. Therefore, the high value of residual VM, should not be all attributed to incomplete pyrolysis of the organic matter.

In the case of co-pyrolysis, results illustrated in Table 3 show a decrease in FC content and an increase in ash content for CC-PGP500. The inverse tendency is observed for CC-PC500. However, VM content illustrated a decline for both samples compared to the calculated results.

The ultimate analyses of biochar from the pyrolysis at 500 °C (Table 3) shows a high C content for PGP500 (79.23 wt%) and PC500 (75.42 wt%). As can be seen, both samples have high HHV of ~26 MJ/

Table 3
Main characteristics of the obtained biochar samples.

	CC500	PC500	PGP500	CC-PC500 (Experimental)	CC-PC500 (Expected)	CC-PGP500 (Experimental)	CC-PGP500 (Expected)
Proximate analysis (wt%)							
Moisture	1.3	0.9	1.3	1.8	1.1	1.70	1.3
VM	32.0	17.8	18.9	26.1	24.9	22.8	25.5
FC	32.9	79.1	72.5	52.9	56.0	61.7	52.7
Ash	33.5	9.2	7.3	19.2	17.9	13.8	20.4
pH	11.0	7.8	8.1	8.4	9.4	8.6	9.5
EC (mS/cm)	11.0	1.0	1.9	0.8	6.0	0.78	6.4
Ultimate analysis (wt%)							
C	46.3	75.4	79.2	51.3	60.9	58.5	62.8
H	1.7	2.7	2.4	1.4	2.2	1.6	2.1
N	1.8	0.1	0.7	0.1	0.9	0.3	1.2
S	0.3	0.0	0.0	0.0	0.2	0.0	0.2
O*	16.4	21.8	17.7	25.3	19.1	25.9	17.0
Fuel properties							
HHV(MJ/kg)	15.87	25.85	26.75	17.5	20.86	19.91	21.31
H/C	0.44	0.42	0.37	0.37	0.43	0.38	0.41
O/C	0.27	0.22	0.17	0.37	0.25	0.30	0.22
Fuel ratio (*Fr*)	1.03	4.44	3.83	2.03	2.74	2.70	2.43
Thermal stability (*Ts*)	0.51	0.82	0.79	0.67	0.67	0.73	0.65
Mineral concentration (ppm)							
Ca	36,000	1140	2840	41,100	18,600	38,800	19,500
Mg	5600	1960	870	9570	3800	8990	3260
K	13,200	9200	29,500	35,000	11,200	42,100	21,370
Na	170	560	600	160	360	3100	390
P	650	840	1490	1000	750	1400	1070
Fe	380	180	64	160	280	140	220
Al	260	750	1170	390	500	250	190

(*) by difference.

Kg. In contrast, CC500 has low C content (46.32 wt%) and HHV (15.87 MJ/Kg) and high N content (1.75 wt%).

Co-pyrolysis tests show a decline in HHV, C, H and N contents and an increase in O content for both co-pyrolysis samples, compared to single bio-chars.

The atomic H/C and O/C ratios of the biochars produced in the pyrolysis and co-pyrolysis experiments are represented Table 3**.** The relation between both ratios are plotted using the Van Krevelen diagram (Fig. 2). These ratios offer insights into the degree of thermochemical conversion during dehydration and carbonization reactions. Compared to biomass feedstocks, which are in the region typical for biomass, lower H/C and O/C ratios are observed in biochars, which is an obvious consequence of the pyrolysis induced carbonization process. This decline reflects the loss of O-containing functional groups, resulting in higher stability [79] and lower hydrophilicity. It should be noticed that the lowest H/C and O/C molar ratios are indicative of the high quality of the biochar as a solid fuel. According to IBI Guidelines [80], biochars with H/C < 0.7 and O/C < 0.4 are also effective in C sequestration when added to the soil.

The differences between the experimental and theoretical results for co-pyrolysis can be attributed to the catalytic activity of the metals in the CC ash fraction namely Ca, K and Mg (Table 2), which favor synergetic effects. These results are consistent with those reported by several studies using different raw materials including date palm branches and wastewater microalgae [81], bamboo and microalgae [78], tobacco stem and corn stalk [69].

Mineral composition of the obtained biochar derived pyrolysis and co-pyrolysis are shown in Table 3. CC500 biochar contains high concentrations of Ca and Mg compared to PC500 and PGP500. Comparing these values, it can be observed that co-pyrolysis CC-PGP500 biochar is enriched with minerals, in the order K> Ca> Mg, while for CC-PC500 the order is Ca> K> Mg. The relative content of Na, Fe, P and Al, instead, decreases compared to single pyrolysis biochars. Altogether, however, all biochars have a high content of AAEMs, which makes them interesting for a range of applications. For instance, mineral components such as Ca, Mg, K and P can enable biochar to provide a direct supply of mineral nutrients, thus promoting plant growth. Likewise, the high amount of Ca and Mg, in particular, are crucial for improving soil structure and neutralizing acidity. In a further example, anions like OH^-, CO_3^{2-} and PO_4^3 released from biochar minerals, have a significant role in the removal of heavy metals by the formation of metal precipitates [82]. As another application, the availability of minerals in biochar can lead to enhance sorption of organic contaminants, in particular polar and ionic organic compounds [83]. This may be ascribed to several mechanisms including organic functional groups complexation, metal ion exchange, mineral precipitation and Cation-π interactions. It has been previously claimed that precipitation and cation exchange are due to the inorganic minerals present in the biochar, whereas complexation and Cation-π interactions are assigned to the organic fraction.

The quality of the biochar can be determined also by fuel parameters such the *Fr* and the *Ts*. According to Selvarajoo et al [27], high *Fr* values are indicative of greater fuel ignition difficulties and slower combustion, resulting in more unburnt carbon and potentially affecting combustion efficiency. Alternatively, solid fuels having lower *Fr* exhibit better flame stability, higher carbon burn-up and greater combustibility, although they may cause unintended ignition during the storage process. According to Selvarajoo et al. [40], the *Fr* for different coals is $\geq$10 for anthracite, 6–10 for semi-anthracite, 3–6 for semi-bituminous, and $<$3 for bituminous and sub-bituminous. As expected, all biochars have higher *Fr* than the parent biomass, as a consequence of carbonisation. CC500 the lowest *Fr* value of 1.03. PC500 and PGP500 have, instead, *Fr* values larger than 3 and can be classified as semi-bituminous. Co-pyrolysis biochars have *Fr* of 2–2.7, which allows to classify them as sub-bituminous.

The CC500 biochar has the lowest thermal stability; instead, PC500 and PGP500 are more thermally stable, with *Ts* close to 1. This can be reconduced to the lower lignin content of CC compared to PC and PGP samples. Previous studies explained, indeed, that thermal stability depends on the content of cellulose, hemicellulose and lignin. Lignin-rich biomass has better thermal stability due to its complex structure, decomposing over a wide temperature range from 200 to 900 °C [40,84,85]. Hemicellulose is less thermally stable than cellulose, and both decompose at temperatures below 450 °C [86]. The observed decline in *Fr* and *Ts* is in agreement with the study of Egbosiuba et al. [86].

3.2.3. pH and EC

Results of pH and EC for biochar samples are seen in Table 3. Compared to results of the original biomasses, biochars derived pyrolysis, pH increase with temperature and the high value is shown for CC500 (10.95) followed by PGP500 (8.10) and PC500 (7.81). The high pH values can be attributed to the biomass high ash content, which can be alkaline in nature, the higher carbonate content, the separation of alkaline salts from organic matter, the lower carboxyl group content and the higher number of functional oxygen groups as pyrolysis temperature increases [87].

The EC of biochars derived pyrolysis (Table 3) increases compared to the raw biomasses. The values are in the order of CC500> PGP500> PC500. Some dissolvable salts decomposed during the pyrolysis process explain the increase of EC. The breakdown of certain organic structures by pyrolysis also resulted in an overall increase in their solubilisation.

Very remarkable synergetic effects of co-pyrolysis can be seen in the EC values. The co-pyrolysis derived biochars showed an alkaline nature with the addition of CC to PGP/PC, which presented an increase compared to PC500 and PGP500. This trend could be assigned to the high content of inorganic elements (Ca, K, Mg, etc.) and the formation of different inorganic alkalis and carbonate salts, like KCl, KOH, $MgCO_3$, $CaCO_3$, etc. However, the inverse tendency is observed for EC and this could be due to the decline of carbonate concentration compared to the CC500.

In terms of application, the addition of alkaline biochar can boost soil pH, which in turn leads to a liming effect, thereby neutralizing acidic soils. In addition, increasing the pH in acid soils affects the bioavailability of toxic elements. It can also stimulate microbial activity and, consequently, plant growth and productivity can be improved [82].

3.2.4. Biochar surface functionalities

Further insight into the properties of the biochars could be derived from the results of FTIR and XRD analysis. FTIR spectra of the pyrolysis and co-pyrolysis biochars are illustrated in Fig. 3**b**. It can be observed that functional groups decrease upon pyrolysis [88], which is consistent with the changes in proximate and elemental analysis. The O—H stretching peak (between 300 and 3600 cm^{-1} in raw materials spectra) decreases in biochars spectra due to the moisture evaporation, which breaks down hydroxyl groups of the aliphatic chain in the temperature range from 120 to 200 °C [89]. The aliphatic C—H stretching peak (2920 cm^{-1}) intensity decreases indicates a loss of labile aliphatic structures upon thermal cracking. In addition, it could be due to the occurrence of demethoxylation, demethylation, and dehydration of lignin [90]. The carboxylic acids COOH band observed at 1614 cm^{-1}, diminishes in intensity and then becomes negligible. The peak at ~1690 cm^{-1} corresponds to the carbonyl and carboxyl groups of carbohydrates, ketones and aldehydes, with possibly small amounts of amides. The aromatic ring stretching vibrations of C=C were identified at ~1570 cm^{-1}. For C—H and CH_2, the peak at ~1410 cm^{-1} attributed stretching vibrations in the aliphatics of PC500 and PGP500 samples. The band at 1180–1220 cm^{-1} is assigned to phenolic OH and aromatic C—O bonds. The slight vibrations of C—H bonds in the heteroaromatic and aromatic compounds are noticeable at 530–870 cm^{-1} [91]. With the CC addition, a pronounced peak in the region around 1418 cm^{-1} is still present. This peak is associated with carbonate (CO_3^{2-}), existed in the CC

sample. Likewise, the relative intensity of the peak at 872 cm^{-1} becomes more intense with the addition of CC to PC and PGP, which further confirms that this peak may be attributed to CO_3^2. These data agree with the mineral composition results (Table 3).

XRD patterns of the obtained biochars are given in Fig. 3**d**. The results show that upon pyrolysis some new peaks appear compared to the biomass feedstocks, while other completely disappear. A sharp peak at $2\theta = 23.4°$ can be seen in the CC-PC500 sample, indicating the formation of aromatic C structures [92]. This peak is not present in the CC-PGP500 sample. Other sharp peaks at $2\theta = 28.78°$ and 29.71 indicate the formation of sylvite (KCl) and calcium carbonate ($CaCO_3$) in both biochars. CC-PC500 is formed from 55 % of coesite (SiO_2), 39 % of calcite, magnesian (Mg0.1 Ca0.9 CO_3) and 6 % of sylvite (KCl). The formation of calcite contributes to the alkalinity of the studied biochars, which is confirmed by the pH results [93]. More minerals are present in CC-PC500 than in CC-PGP500. The XRD spectra show approximatively the same peaks at 36.40, 39.78, 40.80, 43.55, 47.77 and 48.85°, which are associated to the mineral crystals such as MgO, $CaSO_4$, KCl (sylvite), SiO_2, $CaCO_3$ and Na_4SiO_4 in the obtained biochars. From these results and after CC addition, the XRD of biochar samples indicates the presence of wide range of mineral elements, which is consistent with several studies highlighting that co-pyrolysis process, affects the structure and chemical composition of biochars [15,49,81].

3.3. Bio-oil GC–MS

Numerous compounds have been identified in the bio-oil samples. These compounds have been classified according to their functional groups into aromatic, O-aromatic, phenol, aliphatic, O-aliphatic, N-aliphatic, furfural, furan, pyran, anhydrosugar, sugar-derivate, naphthalene and vitamin E compounds, retene, retene deriv. Results of the obtained bio-oils are given in Fig. 6 as area %. The stars in the figure indicate the values calculated for the co-pyrolysis experiments under the assumption that interactions between the biomasses are negligible. The detailed composition of the produced bio-oils is shown **Table S1-S5**.

The individual pyrolysis of CC, PGP and PC at 500 °C leads to bio-oils with different composition. CC generates bio-oil rich with aliphatics (37.4 %), phenols (33.2 %), O-aliphatics (3.9 %) and naphthalene (3.2 %). Phenols result mainly from the cracking of lignin, O-containing species from degradation of cellulose and hemicellulose [44]. The aliphatic compounds present in CC are mainly coming from the breakdown of lipids [78] and N-containing compounds are mainly derived from the decomposition of proteins present in CC biomass [44].

The bio-oil from PGP is largely composed of furfural (58.1 %), anhydrosugars (25.3 %), sugar-derivates (8.1 %) and oxygenated aromatic compounds (4.5 %). These results are in good agreement with those reported in literature [43]. The furfural and anhydrosugars are mainly produced from cellulose and hemicellulose [43].

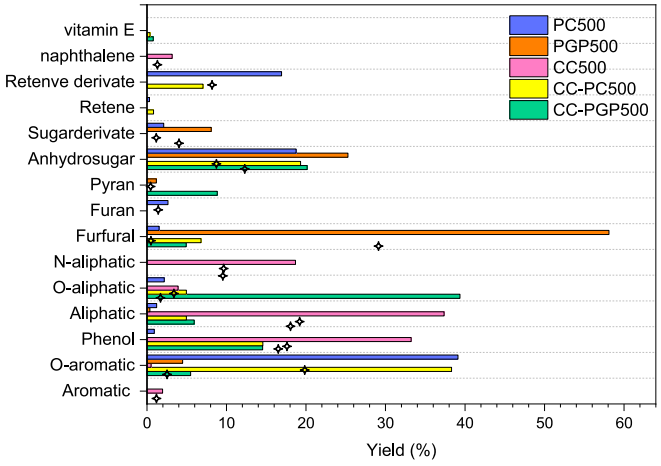

Fig. 6. Pyrolytic bio-oil compounds obtained from pyrolysis and co-pyrolysis (stars: expected results).

PC bio-oil contains a high fraction of oxygenated aromatics (39.1 %), anhydrosugars (18.8 %) and retene derivates (16.9 %). Retene (1-methyl-7-isopropylphenanthrene) is a methylated tricyclic aromatic compound with the basic skeleton of phenanthrene. It is mainly a thermal degradation product of the resin diterpenoids in softwood [94]. The high value of aromatic compounds is due to the high amount of lignin present in PC biomass. These results are in good agreement with those reported for woody biomasses (catalytic upgrading of intermediate pyrolysis bio-oil to hydrocarbon-rich liquid biofuel via a novel two-stage solvent-assisted process).

Comparison of the co-pyrolysis oils with the oils obtained from single biomass pyrolysis and with the expected values (denoted by the stars) reveals important synergetic effects, even though the overall pyrolysis degree was not changed (as confirmed by unaltered char yields). Notably no new compounds are formed during the co-pyrolysis of biomasses, the relative amounts of the different species are severely affected.

The CC-PGP500 bio-oil is found to contain much more O-aliphatics (39,4%), anhydrosugars (20.1 %) and O-aromatics (5.5 wt%) than would be expected. Likewise, the oil from CC-PC500 co-pyrolysis contained much more anhydrosugars (19.3 %) and O-aromatics (38.3 %) than expected.

The content of Phenol decreases in the co-pyrolysis bio-oils. For CC-PGP500 it is worth noting the decrease of furfural and the presence of 5-hydroxymethyl, which is generated from polysaccharides breakdown. In CC-PC the decrease of retene derivatives can be noticed, which is a good upgrading of the pyrolytic bio-oil. These observations suggest that during co-pyrolysis.

the presence of certain minerals present in CC, such as alkali metals (Na and K) has an effect on the break down of the biomass building blocks, indeed K, in particular K, has been reported to favour conversion of anhydrosugars into linear aldehydes, and 5-hydroxymethyl furfural [25]. Several studies highlighted, also, the possibility of interaction during co-pyrolysis between the primary volatiles produced from the different components of the biomasses. For instance, it has been reported that during pyrolysis, biomass rich with lipids, proteins and carbohydrates like CC biomass can affect the nitrogen content of co-pyrolysis bio-oils. Chang et al. [1] reported that co-pyrolysis of palm kernel shell and Nannochloropsis sp. improved aromatics content. In our study, due to the complex components of CC biomass, which contains carbohydrates, proteins and lipids, the co-pyrolysis mechanism cannot be easily disclosed.

For all the bio-oil samples it can be observed that O-containing compounds are abundant, in relation to the high O content in all the three biomasses [78]. Pyrolysis oils are not suitable for use as fuel without a hydro-de-oxygenation treatment. The produced oils could, alternatively be used for production of chemicals, asphalt binders, bioplastics, carbonaceous materials, pesticides and fertilizers [95]. Indeed, the bio-oil derived from CC-PC500 pyrolysis is very rich in aromatic compounds (O-aromatics and phenol), which could be transformed into value-added fuels or used directly as useful chemicals [96]. This aromatic-rich bio-oil could be hydro-treated into cycloalkanes and aromatic hydrocarbons. The benzenes and phenolic compounds could be used for the preparation of products such as synthetic resins, dyes, pesticides, lubricating oils, solvents, etc. [43]. In addition, the bio-oil derived from the pyrolysis of CC-PGP500, which is rich in aliphatic compounds and anhydrosugars could be used to produce different types of sugars such as glucose by hydrolysis.

4. Conclusion

Results of co-pyrolysis experiments of cactus cladodes (CC) with pinecones (PC) and pomegranate peels (PGP) show an interesting effect

in terms of quality and yields of pyrolysis products, in particular, bio-oil yields are enhanced, at the expense of gas yields.

The char yields are not affected and the gas yields even decrease at the advantage of oil. The low contact time between solid and volatiles in the tubular reactor configuration, and the low temperature, which keeps most mineral matter into the solid, may be the key to the negligible enhancement of pyrolysis rates. In particular, the very high Ca content of CC does not explicate its potential catalytic activity because at 500 °C it remains in the form of carbonates (higher temperature would be needed for it to calcine into the more active CaO).

CC does have, instead, an effect on the quality of the bio-oil, both in terms of yield and composition Indeed, it increases the share of aromatics and of phenols, while it decreases primary pyrolysis products such as furfural, anhydrosugars and retene derivatives. This may suggest the existence of interactions between the different components of the biomasses, lipids, proteins etc.

Remarkable effects are observed as regards the pH and EC of co-pyrolysis biochars. Accordingly, these biochars are suitable for amendment and remediation of degraded acidic soils. They also have potential for increasing C storage in soils due their high stability and high C content. The effect on biochars alkalinity can be reconduced to the richness of AAEMs in CC biomass.

Further investigation is needed to examine how processing conditions, mixing ratio, volatiles-char contact time affect co-pyrolysis results. It is also recommended to examine the effects of biochar obtained on various soils and plant growth.

CRediT authorship contribution statement

Assia Maaoui: Writing – original draft, Visualization, Validation, Software, Methodology, Investigation, Formal analysis, Data curation, Conceptualization. **Raouia Chagtmi:** Writing – original draft, Visualization, Validation, Software, Methodology, Investigation, Formal analysis, Conceptualization. **Francesca Cerciello:** Writing – review & editing, Visualization, Validation, Methodology. **Aida Ben Hassen Trabelsi:** Supervision. **Fernando Stanzione:** Methodology. **Maria Maddalena Oliano:** Methodology. **Osvalda Senneca:** Writing – review & editing, Visualization, Validation, Supervision, Methodology, Investigation. **Barbara Apicella:** Writing – review & editing, Supervision, Resources.

Declaration of competing interest

The authors declare that they have no known competing financial interests or personal relationships that could have appeared to influence the work reported in this paper.

Appendix A. Supplementary data

Supplementary data to this article can be found online at https://doi.org/10.1016/j.tsep.2025.103651.

Data availability

No data was used for the research described in the article.

References

[1] WBA, Global Bioenergy Statistics 2021 World Bioenergy Association, (2021).

[2] A.I. Osman, M. Farghali, I. Ihara, A.M. Elgarahy, A. Ayyad, N. Mehta, K.H. Ng, E. M. Abd El-Monaem, A.S. Eltaweil, M. Hosny, S.M. Hamed, S. Fawzy, P.S. Yap, D. W. Rooney, Materials, fuels, upgrading, economy, and life cycle assessment of the pyrolysis of algal and lignocellulosic biomass: a review, Environ. Chem. Lett. J. (2023) 1–58, https://doi.org/10.1007/s10311-023-01573-7.

[3] V. Dhyani, T. Bhaskar, A comprehensive review on the pyrolysis of lignocellulosic biomass, Renew. Energy 129 (2018) 695–716, https://doi.org/10.1016/j.renene.2017.04.035.

[4] S. Yu, L. Wang, Q. Li, Y. Zhang, H. Zhou, Sustainable carbon materials from the pyrolysis of lignocellulosic biomass, Mater. Today Sustainability 19 (2022), https://doi.org/10.1016/j.mtsust.2022.100209.

[5] Y. K N, P.D. T, S. P, K. S, Y.K. R, S. Varjani, S. AdishKumar, G. Kumar, R.B. J, Lignocellulosic biomass-based pyrolysis: A comprehensive review, Chemosphere 286 (2022), https://doi.org/10.1016/j.chemosphere.2021.131824.

[6] A.I. Osman, Z.Y. Lai, M. Farghali, C.L. Yiin, A.M. Elgarahy, A. Hammad, I. Ihara, A. S. Al-Fatesh, D.W. Rooney, P.S. Yap, Optimizing biomass pathways to bioenergy and biochar application in electricity generation, biodiesel production, and biohydrogen production, Environ. Chem. Lett. 21 (2023) 2639–2705, https://doi.org/10.1007/s10311-023-01613-2.

[7] T. Kan, V. Strezov, T.J. Evans, Lignocellulosic biomass pyrolysis: A review of product properties and effects of pyrolysis parameters, Renew. Sustain. Energy Rev. 57 (2016) 1126–1140, https://doi.org/10.1016/j.rser.2015.12.185.

[8] C.Z. Zaman, K. Pal, W.A. Yehye, S. Sagadevan, S.T. Shah, G.A. Adebisi, E. Marliana, R.F. Rafique, R. Bin Johan, Pyrolysis: A Sustainable Way to Generate Energy from Waste, in: Pyrolysis, InTech, 2017. doi: 10.5772/intechopen.69036.

[9] A. Tursi, A review on biomass: Importance, chemistry, classification, and conversion, Biofuel Res. J. 6 (2019) 962–979, https://doi.org/10.18331/BRJ2019.6.2.3.

[10] W.H. Chen, C. Naveen, P.K. Ghodke, A.K. Sharma, P. Bobde, Co-pyrolysis of lignocellulosic biomass with other carbonaceous materials: A review on advance technologies, synergistic effect, and future prospectus, Fuel 345 (2023), https://doi.org/10.1016/j.fuel.2023.128177.

[11] W. Wang, R. Lemaire, A. Bensakhria, D. Luart, Review on the catalytic effects of alkali and alkaline earth metals (AAEMs) including sodium, potassium, calcium and magnesium on the pyrolysis of lignocellulosic biomass and on the co-pyrolysis of coal with biomass, J. Anal. Appl. Pyrol. 163 (2022), https://doi.org/10.1016/j.jaap.2022.105479.

[12] T.A. Vo, Q.K. Tran, H.V. Ly, B. Kwon, H.T. Hwang, J. Kim, S.S. Kim, Co-pyrolysis of lignocellulosic biomass and plastics: A comprehensive study on pyrolysis kinetics and characteristics, J. Anal. Appl. Pyrol. 163 (2022), https://doi.org/10.1016/j.jaap.2022.105464.

[13] D. Rathnayake, P.O. Ehidiamhen, C.E. Egene, C.V. Stevens, E. Meers, O. Mašek, F. Ronsse, Investigation of biomass and agricultural plastic co-pyrolysis: Effect on biochar yield and properties, J. Anal. Appl. Pyrol. 155 (2021), https://doi.org/10.1016/j.jaap.2021.105029.

[14] B.B. Uzoejinwa, X. He, S. Wang, A. El-Fatah Abomohra, Y. Hu, Q. Wang, Co-pyrolysis of biomass and waste plastics as a thermochemical conversion technology for high-grade biofuel production: Recent progress and future directions elsewhere worldwide, Energy Convers Manag. 163 (2018) 468–492, https://doi.org/10.1016/j.enconman.2018.02.004.

[15] D.O. Usino, P. Ylitervo, T. Richards, Primary products from fast co-pyrolysis of palm kernel shell and sawdust, Molecules 28 (2023), https://doi.org/10.3390/molecules28196809.

[16] Y. Nie, M. Deng, M. Shan, X. Yang, Is there interaction between forestry residue and crop residue in co-pyrolysis? Evidence from wood sawdust and peanut shell, J. Therm. Anal. Calorim. 148 (2023) 2467–2481, https://doi.org/10.1007/s10973-022-11910-7.

[17] A.K. Varma, N. Lal, A.K. Rathore, R. Katiyar, L.S. Thakur, R. Shankar, P. Mondal, Thermal, kinetic and thermodynamic study for co-pyrolysis of pine needles and styrofoam using thermogravimetric analysis, Energy 218 (2021), https://doi.org/10.1016/j.energy.2020.119404.

[18] N.A. Rajput, M. Laghari, H. ur, R. Mangio, R.K. Soothar, Enhanced phosphorus and potassium recovery through co-pyrolysis of nutrient-rich biomass feedstocks for engineered biochar production, Bioresour. Technol. Rep. 26 (2024), https://doi.org/10.1016/j.biteb.2024.101818.

[19] A. Maaoui, R. Chagtmi, G. Lopez, M. Cortazar, M. Olazar, A.B.H. Trabelsi, Impact of pyrolysis process conditions on the features of the biochar from Opuntia ficus indica fruit peels, Biomass Convers. Biorefin. (2024), https://doi.org/10.1007/s13399-024-05750-8.

[20] A. Maaoui, A. Ben Hassen Trabelsi, M. Hamdi, R. Chagtmi, F. Jamaaoui, G. Lopez, M. Cortazar, M. Olazar, Towards local circular economy through Opuntia Ficus Indica cladodes conversion into renewable biofuels and biochars: Product distribution and kinetic modelling, Fuel 332 (2023) 126056, https://doi.org/10.1016/j.fuel.2022.126056.

[21] J. Alvarez, G. Lopez, M. Amutio, J. Bilbao, M. Olazar, Physical activation of rice husk pyrolysis char for the production of high surface area activated carbons, Ind. Eng. Chem. Res. 54 (2015) 7241–7250, https://doi.org/10.1021/acs.iecr.5b01589.

[22] L. Zou, X. He, W. Yang, H. Shao, Y. Wang, Q. Zhao, Co-pyrolysis of peanut shell with municipal sludge: reaction mechanism, product distribution, and synergy, Environ. Sci. Pollut. Res. 30 (2023) 94081–94096, https://doi.org/10.1007/s11356-023-28992-x.

[23] Y. Liu, Y. Song, J. Fu, W. Ao, A. Ali Siyal, C. Zhou, C. Liu, M. Yu, Y. Zhang, J. Dai, X. Bi, Co-pyrolysis of sewage sludge and lignocellulosic biomass: Synergistic effects on products characteristics and kinetics, Energy Convers Manag. 268 (2022), https://doi.org/10.1016/j.enconman.2022.116061.

[24] L. Ali, A. Palamanit, K. Techato, A. Khurshid, W.J. Baloch, Valorization of rubberwood sawdust and sewage sludge by pyrolysis and co-pyrolysis using agitated bed reactor for producing biofuel or value-added products, Environ. Sci. Pollut. Res. (2022), https://doi.org/10.1007/s11356-021-15283-6/Published.

[25] A. Bhatnagar, R. Barthen, H. Tolvanen, J. Konttinen, Bio-oil stability through stepwise pyrolysis of groundnut shells: Role of chemical composition, alkali and alkaline earth metals, and storage conditions, J. Anal. Appl. Pyrol. 157 (2021) 105219, https://doi.org/10.1016/j.jaap.2021.105219.

[26] A. Tomczyk, Z. Sokołowska, P. Boguta, Biochar physicochemical properties: pyrolysis temperature and feedstock kind effects, Rev. Environ. Sci. Biotechnol. 19 (2020) 191–215, https://doi.org/10.1007/s11157-020-09523-3.
[27] W. Saadi, S. Rodríguez-Sánchez, B. Ruiz, S. Souissi-Najar, A. Ouederni, E. Fuente, Pyrolysis technologies for Pomegranate (Punica 1 granatum L.) peel wastes. Prospects in the 2 Bioenergy Sector, 2019.
[28] I. Akkari, Z. Graba, N. Bezzi, F.A. Merzeg, N. Bait, A. Ferhati, Raw pomegranate peel as promise efficient biosorbent for the removal of Basic Red 46 dye: equilibrium, kinetic, and thermodynamic studies, Biomass Convers. Biorefin. 13 (2023) 8047–8060, https://doi.org/10.1007/s13399-021-01620-9.
[29] S. Rafiaee, M.R. Samani, D. Toghraie, Removal of hexavalent chromium from aqueous media using pomegranate peels modified by polymeric coatings: Effects of various composite synthesis parameters, Synth. Met. 265 (2020), https://doi.org/10.1016/j.synthmet.2020.116416.
[30] N. Rouahna, D. Ben Salem, I. Bouchareb, A. Nouioua, A. Ouakouak, A. Fadel, N. Hamdi, R. Boopathy, Reduction of crystal violet dye from water by pomegranate peel–derived efficient biochar: influencing factors and adsorption behaviour, Water Air Soil Pollut. 234 (2023), https://doi.org/10.1007/s11270-023-06338-0.
[31] N.D. Shooto, Application of carbon from pomegranate husk for the removal of ibuprofen, cadmium and methylene blue from water, Heliyon 9 (2023), https://doi.org/10.1016/j.heliyon.2023.e20268.
[32] S. Ben-Ali, I. Jaouali, S. Souissi-Najar, A. Ouederni, Characterization and adsorption capacity of raw pomegranate peel biosorbent for copper removal, J. Clean. Prod. 142 (2017) 3809–3821, https://doi.org/10.1016/j.jclepro.2016.10.081.
[33] P. Gullón, G. Astray, B. Gullón, I. Tomasevic, J.M. Lorenzo, Pomegranate peel as suitable source of high-added value bioactives: tailored functionalized meat products, Molecules 25 (2020), https://doi.org/10.3390/molecules25122859.
[34] F. Azmat, M. Safdar, H. Ahmad, M.R.J. Khan, J. Abid, M.S. Naseer, S. Aggarwal, A. Imran, U. Khalid, S.M. Zahra, F. Islam, S.A. Cheema, U. Shehzadi, R. Ali, A. B. Kinki, Y.A. Ali, H.A.R. Suleria, Phytochemical profile, nutritional composition of pomegranate peel and peel extract as a potential source of nutraceutical: A comprehensive review, Food Sci. Nutr. (2024), https://doi.org/10.1002/fsn3.3777.
[35] J. Alvarez, M. Amutio, G. Lopez, J. Bilbao, M. Olazar, Fast co-pyrolysis of sewage sludge and lignocellulosic biomass in a conical spouted bed reactor, Fuel 159 (2015) 810–818, https://doi.org/10.1016/j.fuel.2015.07.039.
[36] S. Hongthong, W. Sangsida, S. Wongcharee, A. Chanthakhot, P. Aungthitipan, K. Suwannahong, T. Kreetachat, J. Rioyo, Enhanced biochar production via co-pyrolysis of biomass residual with plastic waste after recycling process, Int. J. Chem. Eng. 2024 (2024), https://doi.org/10.1155/2024/1176275.
[37] R.K. Mishra, Co-pyrolysis of low-value wood sawdust and non-recyclable plastics into char: effect of plastic loading on char yield and its properties, RSC Sustain. (2025), https://doi.org/10.1039/d4su00739e.
[38] E. David, J. Kopac, Valorization of poultry manure into biochar, bio-oil and gas product by co-pyrolysis with residual biomass and the effects analysis of the feedstock on products yield and their characteristics, J. Anal. Appl. Pyrol. 186 (2025), https://doi.org/10.1016/j.jaap.2025.106978.
[39] Senneca2018, (n.d.).
[40] A. Selvarajoo, Y.L. Wong, K.S. Khoo, W.H. Chen, P.L. Show, Biochar production via pyrolysis of citrus peel fruit waste as a potential usage as solid biofuel, Chemosphere 294 (2022), https://doi.org/10.1016/j.chemosphere.2022.133671.
[41] C. Sheng, J.L.T. Azevedo, Estimating the higher heating value of biomass fuels from basic analysis data, Biomass Bioenergy 28 (2005) 499–507, https://doi.org/10.1016/j.biombioe.2004.11.008.
[42] S.A. El-Sayed, M.E. Mostafa, Pyrolysis and co-pyrolysis of Egyptian olive pomace, sawdust, and their blends: Thermal decomposition, kinetics, synergistic effect, and thermodynamic analysis, J. Clean. Prod. 401 (2023), https://doi.org/10.1016/j.jclepro.2023.136772.
[43] W. Saadi, S. Rodríguez-Sánchez, B. Ruiz, S. Souissi-Najar, A. Ouederni, E. Fuente, Pyrolysis technologies for pomegranate (Punica granatum L.) peel wastes, in: Renew. Energy, 136, 2019, pp. 373–382, https://doi.org/10.1016/j.renene.2019.01.017.
[44] P. Cross, C. Mukarakate, M. Nimlos, D. Carpenter, B.S. Donohoe, J.A. Mayer, J. C. Cushman, B. Neupane, G.C. Miller, S. Adhikari, Fast Pyrolysis of opuntia ficus-indica (prickly pear) and grindelia squarrosa (Gumweed), Energy Fuel 32 (2018) 3510–3518, https://doi.org/10.1021/acs.energyfuels.7b03752.
[45] M. Volpe, J.L. Goldfarb, L. Fiori, Hydrothermal carbonization of Opuntia ficus-indica cladodes: Role of process parameters on hydrochar properties, Bioresour. Technol. 247 (2018) 310–318, https://doi.org/10.1016/j.biortech.2017.09.072.
[46] M.R. Yazdani, N. Duimovich, A. Tiraferri, P. Laurell, M. Borghei, J.B. Zimmerman, R. Vahala, Tailored mesoporous biochar sorbents from pinecone biomass for the adsorption of natural organic matter from lake water, J. Mol. Liq. 291 (2019) 111248, https://doi.org/10.1016/j.molliq.2019.111248.
[47] Y. Chen, L. Wang, M. Zhao, H. Ma, D. Chen, Y. Zhang, J. Zhou, Comparative study on the pyrolysis behaviors of pine cone and pretreated pine cone by using TGA-FTIR and pyrolysis-GC/MS, ACS Omega 6 (2021) 3490–3498, https://doi.org/10.1021/acsomega.0c04456.
[48] R. Mahadevan, S. Adhikari, R. Shakya, K. Wang, D. Dayton, M. Lehrich, S.E. Taylor, Effect of alkali and alkaline earth metals on in-situ catalytic fast pyrolysis of lignocellulosic biomass: a microreactor study, Energy Fuel 30 (2016) 3045–3056, https://doi.org/10.1021/acs.energyfuels.5b02984.
[49] S. Wang, B. Cao, Y. Feng, C. Sun, Q. Wang, A.E.F. Abomohra, S. Afonaa-Mensah, Z. He, B. Zhang, L. Qian, L. Xu, Co-pyrolysis and catalytic co-pyrolysis of Enteromorpha clathrata and rice husk: Toward high-quality products, J. Therm. Anal. Calorim. 135 (2019) 2613–2623, https://doi.org/10.1007/s10973-018-7334-4.
[50] P. Qi, Y. Su, L. Yang, J. Wang, M. Jiang, Y. Xiong, Catalytic pyrolysis of rice husk to co-produce hydrogen-rich syngas, phenol-rich bio-oil and nanostructured porous carbon, Energy 298 (2024), https://doi.org/10.1016/j.energy.2024.131427.
[51] L. Puri, Y. Hu, G. Naterer, Critical review of the role of ash content and composition in biomass pyrolysis, Front. Fuels 2 (2024), https://doi.org/10.3389/ffuel.2024.1378361.
[52] Y. Niu, H. Tan, S. Hui, Ash-related issues during biomass combustion: Alkali-induced slagging, silicate melt-induced slagging (ash fusion), agglomeration, corrosion, ash utilization, and related countermeasures, Prog. Energy Combust. Sci. 52 (2016) 1–61, https://doi.org/10.1016/j.pecs.2015.09.003.
[53] S.A. El-Sayed, M.E. Mostafa, Thermal pyrolysis and kinetic parameter determination of mango leaves using common and new proposed parallel kinetic models, RSC Adv. 10 (2020) 18160–18179, https://doi.org/10.1039/d0ra00493f.
[54] A. Maaoui, A. Ben Hassen Trabelsi, A. Ben Abdallah, R. Chagtmi, G. Lopez, M. Cortazar, M. Olazar, Assessment of pine wood biomass wastes valorization by pyrolysis with focus on fast pyrolysis biochar production, J. Energy Instit. 108 (2023), https://doi.org/10.1016/j.joei.2023.101242.
[55] N. Abdullah, R. Mohd Taib, N.S. Mohamad Aziz, M.R. Omar, N. Md Disa, Banana pseudo-stem biochar derived from slow and fast pyrolysis process, Heliyon 9 (2023), https://doi.org/10.1016/j.heliyon.2023.e12940.
[56] S. Hu, L. Jiang, Y. Wang, S. Su, L. Sun, B. Xu, L. He, J. Xiang, Effects of inherent alkali and alkaline earth metallic species on biomass pyrolysis at different temperatures, Bioresour. Technol. 192 (2015) 23–30, https://doi.org/10.1016/j.biortech.2015.05.042.
[57] Z. Wang, J. Cao, J. Wang, Pyrolytic characteristics of pine wood in a slowly heating and gas sweeping fixed-bed reactor, J. Anal. Appl. Pyrol. 84 (2009) 179–184, https://doi.org/10.1016/j.jaap.2009.02.001.
[58] N. Barka, K. Ouzaouit, M. Abdennouri, M. El Makhfouk, Dried prickly pear cactus (Opuntia ficus indica) cladodes as a low-cost and eco-friendly biosorbent for dyes removal from aqueous solutions, J. Taiwan Inst. Chem. Eng. 44 (2013) 52–60, https://doi.org/10.1016/j.jtice.2012.09.007.
[59] M.T.H. Siddiqui, S. Nizamuddin, N.M. Mubarak, K. Shirin, M. Aijaz, M. Hussain, H. A. Baloch, Characterization and process optimization of biochar produced using novel biomass waste pomegranate peel: a response surface methodology approach, Waste Biomass Valoriz. 10 (2019) 521–532, https://doi.org/10.1007/s12649-017-0091-y.
[60] A. Ait Benhamou, A. Boussetta, M. Nadifiyine, A. Moubarik, Effect of alkali treatment and coupling agent on thermal and mechanical properties of Opuntia ficus-indica cladodes fibers reinforced HDPE composites, Polym. Bull. (2021), https://doi.org/10.1007/s00289-021-03619-8.
[61] M. Oudir, Z. Ait Mesbah, D. Lerari, N. Issad, D. Djenane, Development of eco-friendly biocomposite films based on opuntia ficus-indica cladodes powder blended with gum arabic and xanthan envisaging food packaging applications, Foods 13 (2024), https://doi.org/10.3390/foods13010078.
[62] X. Yang, A. Zheng, Z. Zhao, S. Xia, Y. Fan, C. Zhou, F. Cao, L. Jiang, G. Wei, Z. Huang, H. Li, Overcoming biomass recalcitrance to enhance platform chemical production from soft wood by organosolvolysis coupled with fast pyrolysis, Cellulose 26 (2019) 9687–9708, https://doi.org/10.1007/s10570-019-02757-7.
[63] I. Rojas-Molina, E. Gutiérrez-Cortez, M. Bah, A. Rojas-Molina, C. Ibarra-Alvarado, E. Rivera-Muñoz, A. Del Real, M.D.L.A. Aguilera-Barreiro, Characterization of calcium compounds in opuntia ficus indica as a source of calcium for human diet, J. Chem. 2015 (2015), https://doi.org/10.1155/2015/710328.
[64] T.J. Madera-Santana, L. Vargas-Rodríguez, C.A. Núñez-Colín, G. González-García, V. Peña-Caballero, J.A. Núñez-Gastélum, C. Gallegos-Vázquez, J.R. Rodríguez-Núñez, Mucilage from cladodes of opuntia spinulifera salm-dyck: Chemical, morphological, structural and thermal characterization, CYTA – J. Food 16 (2018) 650–657, https://doi.org/10.1080/19476337.2018.1454988.
[65] G. Bensidhom, A. Ben Hassen Trabelsi, M.A. Mahmood, S. Ceylan, Insights into pyrolytic feedstock potential of date palm industry wastes: Kinetic study and product characterization, Fuel 285 (2021), https://doi.org/10.1016/j.fuel.2020.119096.
[66] M.H. Aissaoui, A.B.H. Trabelsi, S. Abidi, K. Zaafouri, K. Haddad, F. Jamaaoui, J. J. Leahy, W. Kwapinski, Sustainable biofuels and biochar production from olive mill wastes via co-pyrolysis process, Biomass Convers. Biorefin. (2021), https://doi.org/10.1007/s13399-021-01735-z.
[67] R. Kumar Mishra, K. Mohanty, Kinetic analysis and pyrolysis behavior of low-value waste lignocellulosic biomass for its bioenergy potential using thermogravimetric analyzer, Mater. Sci. Energy Technol. 4 (2021) 136–147, https://doi.org/10.1016/j.mset.2021.03.003.
[68] A. Shaaban, S.M. Se, N.M.M. Mitan, M.F. Dimin, Characterization of biochar derived from rubber wood sawdust through slow pyrolysis on surface porosities and functional groups, Procedia Eng. (2013) 365–371, https://doi.org/10.1016/j.proeng.2013.12.193.
[69] J. Bai, G. Huang, C. Qiu, X. Shang, Z. Sun, J. Hu, C. Chang, Preparation of low-nitrogen bio-oil from co-pyrolysis of waste tobacco stem and corn stalk: Product characteristics and denitrogenation mechanism, Energy 301 (2024), https://doi.org/10.1016/j.energy.2024.131653.
[70] H. Yang, R. Yan, H. Chen, D.H. Lee, C. Zheng, Characteristics of hemicellulose, cellulose and lignin pyrolysis, Fuel 86 (2007) 1781–1788, https://doi.org/10.1016/j.fuel.2006.12.013.
[71] J. Aburto, M. Moran, A. Galano, E. Torres-García, Non-isothermal pyrolysis of pectin: A thermochemical and kinetic approach, J. Anal. Appl. Pyrol. 112 (2015) 94–104, https://doi.org/10.1016/j.jaap.2015.02.012.

[72] G. San Miguel, D. Fernández-Olmedilla, F. Sánchez-Godoy, Drying of prickly pear (Opuntia ficus-indica (L.) Miller) and its potential as a solid biofuel, Agronomy 12 (2022), https://doi.org/10.3390/agronomy12092231.
[73] D. Hourlier, Thermal decomposition of calcium oxalate: beyond appearances, J. Therm. Anal. Calorim. 136 (2019) 2221–2229, https://doi.org/10.1007/s10973-018-7888-1.
[74] G. Yildiz, F. Ronsse, R. Venderbosch, R. van Duren, S.R.A. Kersten, W. Prins, Effect of biomass ash in catalytic fast pyrolysis of pine wood, Appl. Catal. B 168–169 (2015) 203–211, https://doi.org/10.1016/j.apcatb.2014.12.044.
[75] N. Rathnayake, S. Patel, I.G. Hakeem, J. Pazferreiro, A. Sharma, R. Gupta, C. Rees, D. Bergmann, J. Blackbeard, A. Surapaneni, K. Shah, Co-pyrolysis of biosolids with lignocellulosic biomass: Effect of feedstock on product yield and composition, Process Saf. Environ. Prot. 173 (2023) 75–87, https://doi.org/10.1016/j.psep.2023.02.087.
[76] P. Giudicianni, V. Gargiulo, C.M. Grottola, M. Alfè, A.I. Ferreiro, M.A.A. Mendes, M. Fagnano, R. Ragucci, Inherent metal elements in biomass pyrolysis: a review, Energy Fuel 35 (2021) 5407–5478, https://doi.org/10.1021/acs.energyfuels.0c04046.
[77] A. Albergamo, A.G. Potortí, G. Di Bella, N. Ben Amor, G. Lo Vecchio, V. Nava, R. Rando, H. Ben Mansour, V. Lo Turco, Chemical characterization of different products from the tunisian opuntia ficus-indica (L.) mill, Foods 11 (2022), https://doi.org/10.3390/foods11020155.
[78] W. Chen, Y. Chen, H. Yang, M. Xia, K. Li, X. Chen, H. Chen, Co-pyrolysis of lignocellulosic biomass and microalgae: Products characteristics and interaction effect, Bioresour. Technol. 245 (2017) 860–868, https://doi.org/10.1016/j.biortech.2017.09.022.
[79] L. Leng, H. Huang, An overview of the effect of pyrolysis process parameters on biochar stability, Bioresour. Technol. 270 (2018) 627–642, https://doi.org/10.1016/j.biortech.2018.09.030.
[80] IBI, Standardized Product Definition and Product Testing Guidelines for Biochar That Is Used in Soil (aka IBI Biochar Standards), 2015. http://www.biochar-international.org/characterizationstandard.
[81] A. Akhtar, I. Jiříček, V. Krepl, A. Mehrabadi, T. Ivanova, Enhancing sustainability: co-pyrolysis of date palm branches and wastewater microalgae for tailored biochar production, Biofuels (2024), https://doi.org/10.1080/17597269.2024.2304957.
[82] C.J. Atkinson, J.D. Fitzgerald, N.A. Hipps, Potential mechanisms for achieving agricultural benefits from biochar application to temperate soils: A review, Plant Soil 337 (2010) 1–18, https://doi.org/10.1007/s11104-010-0464-5.
[83] P. Shrestha, D.D. Chun, K. Kang, A.E. Simson, N.B. Klinghoffer, Role of metals in biochar production and utilization in catalytic applications: a review, Waste Biomass Valoriz. 13 (2022) 797–822, https://doi.org/10.1007/s12649-021-01519-6.
[84] A. Selvarajoo, D. Oochit, Effect of pyrolysis temperature on product yields of palm fibre and its biochar characteristics, Mater. Sci. Energy Technol. 3 (2020) 575–583, https://doi.org/10.1016/j.mset.2020.06.003.
[85] M. Askeland, B. Clarke, J. Paz-Ferreiro, Comparative characterization of biochars produced at three selected pyrolysis temperatures from common woody and herbaceous waste streams, PeerJ 7 (2019), https://doi.org/10.7717/peerj.6784.
[86] T.C. Egbosiuba, Biochar and bio-oil fuel properties from nickel nanoparticles assisted pyrolysis of cassava peel, Heliyon 8 (2022), https://doi.org/10.1016/j.heliyon.2022.e10114.
[87] H. Jun Huang, T. Yang, F. Ying Lai, G. Qiang Wu, Co-pyrolysis of sewage sludge and sawdust/rice straw for the production of biochar, J. Anal. Appl. Pyroly. 125 (2017) 61–68, https://doi.org/10.1016/j.jaap.2017.04.018.
[88] M.K. Rafiq, R.T. Bachmann, M.T. Rafiq, Z. Shang, S. Joseph, R.L. Long, Influence of pyrolysis temperature on physico-chemical properties of corn stover (zea mays l.) biochar and feasibility for carbon capture and energy balance, PLoS One 11 (2016), https://doi.org/10.1371/journal.pone.0156894.
[89] A.Y. Elnour, A.A. Alghyamah, H.M. Shaikh, A.M. Poulose, Effect of pyrolysis temperature on biochar microstructural evolution , physicochemical characteristics , and its influence on biochar / polypropylene, Composites (2019) 7–9, https://doi.org/10.3390/app9061149.
[90] Y. Wang, Y. Hu, X. Zhao, S. Wang, G. Xing, Comparisons of biochar properties from wood material and crop residues at different temperatures and residence times, Energy Fuel 27 (2013) 5890–5899, https://doi.org/10.1021/ef400972z.
[91] R.R. Domingues, P.F. Trugilho, C.A. Silva, I.C.N. A, C.A. Melo, Z.M. Magriotis, M.A. Sa, D. Melo, Properties of biochar derived from wood and high-nutrient biomasses with the aim of agronomic and environmental benefits, (2017) 1–19.
[92] X. Ying Zhou, F. Xie, M. Jiang, L. KE-ao, S. Ge Tian, Physicochemical properties and lead ion adsorption of biochar prepared from Turkish gall residue at different pyrolysis temperatures, Microsc. Res. Tech. 84 (2021) 1003–1011, https://doi.org/10.1002/jemt.23661.
[93] S. Kloss, F. Zehetner, A. Dellantonio, R. Hamid, F. Ottner, V. Liedtke, M. Schwanninger, M.H. Gerzabek, G. Soja, Characterization of slow pyrolysis biochars: effects of feedstocks and pyrolysis temperature on biochar properties, J. Environ. Qual. 41 (2012) 990–1000, https://doi.org/10.2134/jeq2011.0070.
[94] T. Ramdahl, Retene—a Molecular Marker of Wood Combustion in Ambient Air 306 (5943) (1983) 580-582.
[95] X. Hu, M. Gholizadeh, Progress of the applications of bio-oil, Renew. Sustain. Energy Rev. 134 (2020), https://doi.org/10.1016/j.rser.2020.110124.
[96] H. Wang, Y. Liu, L. Zhang, R. Gunawan, Z. Wang, C.Z. Li, Enrichment of aromatic compounds during the high-pressure reactive distillation of bio-oil, Fuel Process. Technol. 220 (2021), https://doi.org/10.1016/j.fuproc.2021.106897.